

A Theory of Microphase Separation in the Melt of Diblock Copolymers with Smectic Liquid Crystalline Side Groups

Igor I. Potemkin^{*,†,‡} and Anna S. Bodrova[†]

Department of Physics, Moscow State University, Moscow 119992, Russian Federation, and
Department of Polymer Science, University of Ulm, 89069 Ulm, Germany

Received October 21, 2008; Revised Manuscript Received February 6, 2009

ABSTRACT: We develop a theory of microphase separation in a melt of flexible AB block copolymers with liquid crystalline side groups (C) attached to the B block using the strong segregation approximation. Within this theory, we analyze a case when all components of the system are strongly incompatible with each other. We predict thermodynamic stability of two kinds of cylindrical structures having amorphous and liquid crystalline cores, and four kinds of lamellar structures. One of the lamellar structures includes amorphous A and B layers having perpendicular orientations (so-called $A \perp B$ lamellae). Three other kinds have parallel orientations of the layers. Depending on the surface tension coefficient γ_{AC} of the AC interface, either combined BAB amorphous layers alternate with the smectic ones (BAB lamellae) or pure A and B layers are segregated by the smectic ones and their sequence looks like A–B–B–A–B–B... (A–B–B lamellae) or like A–B–A–B... (A–B–A lamellae). Phase diagrams of the system are constructed. Some of the results are compared with experimental data.

1. Introduction

The making of materials with hierarchical (multiscale) spatial order¹ is a challenging direction in modern polymer science. In systems of specially designed block copolymers, the microstructures can have more than one characteristic length scale.^{2–7} The examples of the copolymers revealing two-scale order are comb–coil diblock copolymers,² linear multiblock⁵ and double-grafted^{6,7} copolymers. Other class of systems capable of the two-scale ordering are block copolymers with liquid crystalline (LC) side groups that can covalently^{8–11,14,15} or physically¹⁶ be attached to one of the blocks. In such systems, a competition of liquid crystalline (usually smectic) ordering of the mesogenic side groups and microphase segregation of the blocks is responsible for the morphology of the materials in which the liquid crystalline domains have the length scale in the range of 0.5–5 nm whereas amorphous domains can reach the size of 100 nm. Usually, at low volume fractions of the amorphous (nongrafted) block, hexagonally packed amorphous cylinders have been observed inside a continuous matrix of the blocks with the LC side groups.^{8–12} The LC groups were observed to be oriented parallel to the block copolymer interface and along the axis of the cylinders.^{11,12} Increasing the volume fraction of the amorphous block has been shown to lead to a lamellar structures. In these structures, the LC groups can be oriented either parallel or perpendicular to the block copolymer interface.¹³ At high volume fractions of the amorphous block, LC cylindrical microdomains with the mesogens parallel to the axis of cylinders have been observed.⁸ It has been shown also that the liquid crystalline groups can be efficient to stabilize perpendicular orientation of the amorphous domains (cylinders and lamellae) in thin films.^{9,12,17–21}

In previous theoretical studies of microphase segregation in the system of diblock copolymers with mesogenic side groups in the bulk, the main attention was focused on the order–disorder transitions (both liquid crystalline orientation and microphase segregation) and on the influence of the interaction parameter

between amorphous blocks on phase behavior.^{22,23} In particular, stability of amorphous and liquid crystalline cylindrical domains and lamellae was predicted.

In the present work, we develop a strong segregation theory that takes into account interactions between all species of the system. Within this theory, we predict thermodynamic stability of novel lamellar microstructures with perpendicular orientation of the LC groups to the amorphous layers. Similar structures have been observed in experiment.¹³ Also we perform quantitative comparison of our theoretical results with experimental data obtained in ref 16.

2. Model

Let us consider a melt of AB block copolymers with liquid crystalline side groups. We suppose that both blocks are flexible and consist of identical segments. Following the standard model of polymer chain comprising beads on an immaterial filament,²⁵ each segment (bead) of both blocks is characterized by the excluded volume v , and the average distance between two neighbor beads has the value a . For flexible polymer chains $va^3 \leq 1$ whereas for stiff chains this parameter is much smaller, $va^3 \ll 1$.²⁵ Let N_A and N_B be the numbers of the segments in A and B blocks, respectively. The LC groups (kind C) attached to the B block are modeled as cylindrical rigid rods of the length d and the cross-area σ , Figure 1; $n = d\sigma/v$ being the ratio of the volume of the side group to the excluded volume of the segment. Let us quantify the grafting density of the side groups by fraction $\phi = N_C/N_B$, $0 \leq \phi \leq 1$, where N_C is the number of the groups attached to the B block.

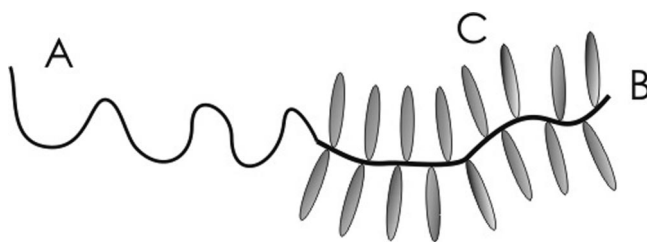


Figure 1. Sketch of the diblock copolymer with liquid crystalline side groups.

*To whom correspondence should be addressed. E-mail: igor@poly.phys.msu.ru.

[†]Department of Physics, Moscow State University.

[‡]Department of Polymer Science, University of Ulm.

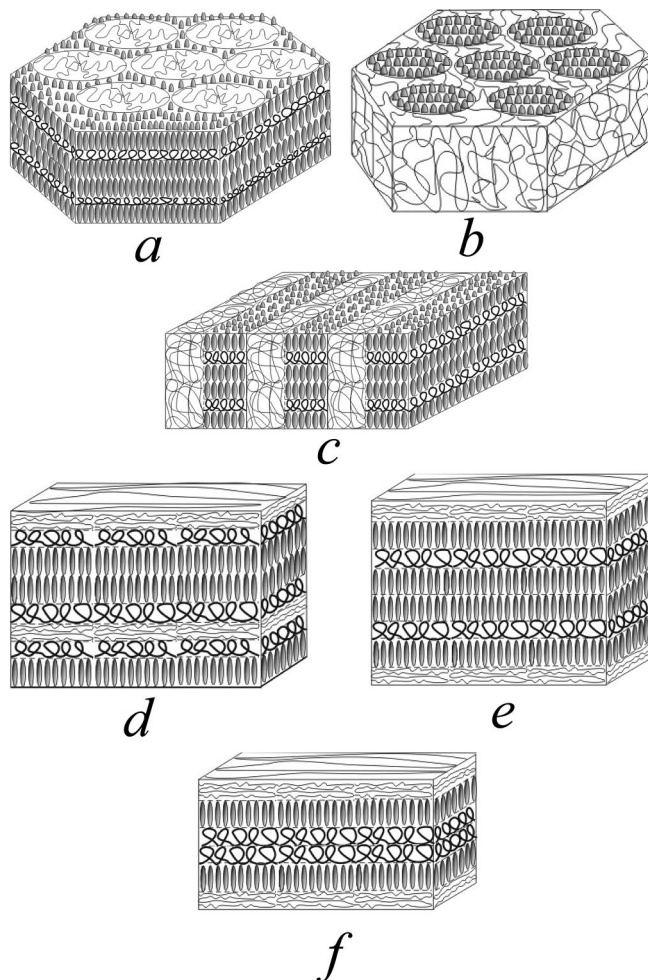


Figure 2. (a) Hexagonally packed amorphous cylinders imbedded in a matrix of alternating smectic and amorphous layers. (b) Hexagonally packed liquid crystalline cylinders (inverse structure). (c) Lamellar structure where amorphous A and B layers have perpendicular orientations ($A \perp B$ lamellae). (d) Combined BAB amorphous layers alternate with the smectic double layers (BAB lamellae). (e) Pure A and B layers are segregated by the smectic layers. The sequence of the amorphous layers looks like $A-B-B-A-B-B \dots$ (A-B-B lamellae). (f) Pure A and B layers are segregated by the smectic layers. The sequence of the amorphous layers looks like $A-B-A-B \dots$ (A-B-A lamellae).

We assume that A, B, and C species are strongly incompatible with each other, and local segregation results in formation of microdomain structures of well defined shape with narrow interfaces (the strong segregation regime). In this regime, the energetic contribution to the total free energy comes from the interfacial energy which is quantified by the surface tension coefficients γ_{AB} , γ_{BC} and γ_{AC} . Here the indexes AB, BC and AC denote respective interfaces. For the sake of convenience, we consider the surface tension coefficients as dimensionless and relation with the dimension ones $\bar{\gamma}_{ij}$ is given by $\gamma_{ij} = \bar{\gamma}_{ij}v/(ak_B T)$, where $k_B T$ is the thermal energy. Let us also assume that in the strong segregation regime the side groups in microdomain structures form smectic layers and the rods have strictly perpendicular orientation to the BC interface. Such assumption is nicely supported by the experimental data^{8,11,12,16} and previous theoretical studies.²³

A competition of the interfacial interactions with the entropic elasticity of the blocks can lead to the formation of various microstructures. The type of the structure depends on the relative lengths of the blocks and fraction of the LC groups, on the interaction parameters, and on the restrictions imposed by the smectic layers of the side groups. That is why we do not expect

that in the strong segregation regime the spherical micelles can be stable because their formation is incompatible with the smectic layering. For the described system, we will examine conditions for the stability of hexagonally packed cylindrical structures with (i) amorphous and (ii) LC cores, Figure 2a,b, (iii) lamellar structure with perpendicular orientations of amorphous A and B layers ($A \perp B$ lamellae), Figure 2c, (iv) lamellar structure where all components form parallel layers and the distance between two BAB amorphous layers is equal to the thickness of double smectic layer (BAB lamellae), Figure 2d, and (v) lamellar structures with parallel layers where A and B amorphous layers are segregated by LC ones and have a sequence $A-B-B-A-B-B \dots$ (A-B-B lamellae), Figure 2e, or $A-B-A-B \dots$ (A-B-A lamellae), Figure 2f. The distance between A and B layers in the structure of Figure 2e corresponds to the thickness of the LC monolayer whereas the distance between two B layers is twice larger.

2.1. Amorphous Cylinders. The amorphous cylindrical structure is modeled as that having a core of the radius R formed by A blocks. The B blocks and C groups occupy a cylindrical layer of the outer radius R_0 (the radius of the Wigner-Seitz cell). It is assumed that the LC groups are oriented parallel to the axis of the cylinder, i.e., they are perpendicular to the BC interfaces, Figure 3a. In addition to the strong incompatibility of B and C species, one more argument in favor of perpendicular orientation of the side groups is radial stretching of the B blocks in the cylindrical structure. The stretching means that there is extra (entropic) attraction between the side groups caused by the B spacers that promotes alignment of the rods. Due to the mixing entropy, a symmetric distribution of the side chains with respect to the backbone (B block) is more favorable, i.e., half of the side groups of each macromolecule forms smectic monolayer above the B layer and half of the groups forms the monolayer below the B layer. The rods of two neighbor macromolecules from different layers do not interpenetrate. Otherwise it would increase radial stretching of the B blocks. The total free energy of the cylindrical structure per chain can be written as a sum of five terms:

$$F_{\text{cyl}}^{\text{amorph}} = F_{\text{int}} + F_{\text{el}}^{\text{A}} + F_{\text{el}}^{\text{B}} + F_{\text{conf}} + F_{\text{mix}} \quad (1)$$

The first term, F_{int} , is an interfacial energy. Its effect is to minimize the number of unfavorable contacts of monomer units of different species with each other:

$$\begin{aligned} \frac{F_{\text{int}}}{k_B T} &= \frac{2\pi R a (h\gamma_{AB} + 2d\gamma_{AC})}{vQ} + \frac{2\pi(R_0^2 - R^2)\gamma_{BC} a}{vQ} \\ &= \gamma_{BC} \phi N_B \frac{a\sigma}{v} + \frac{2a N_A \gamma_{AB} + n\phi \gamma_{AC}}{R(1 + n\phi)} \end{aligned} \quad (2)$$

where h is the thickness of the B layer; Q is the aggregation number of the cylinder per macromolecular monolayer (the layer of the thickness $2d + h$ including one B layer and two smectic monolayers). The second equality in eq. 2 is obtained using dense packing conditions for A, B, and C layers

$$\begin{aligned} (2d + h)\pi R^2 &= Q N_A v, \\ h\pi(R_0^2 - R^2) &= Q N_B v, \\ 2d\pi(R_0^2 - R^2) &= Q N_C d\sigma \end{aligned} \quad (3)$$

which determine the thickness $h = 2v/(\phi\sigma)$ and relations of R with Q and R_0 , $R_0^2/R^2 = 1 + N_B(1 + n\phi)/N_A$. It has to be noticed that minimum possible value of h corresponds to the diameter of the segment (bead) and inequality $h = 2v/(\phi\sigma) \geq (6v/\pi)^{1/3}$ has to be fulfilled. This inequality means that if the cross-area

of the side group is large enough, the value of the fraction ϕ can not reach unity.

The terms F_{el}^A and F_{el}^B in eq 1 are the free energies of radial stretching of A and B blocks. By analogy with the strong segregation approximation for flexible diblock copolymers in the bulk,²⁴ the free energy of stretching of the A block takes the following form:

$$\frac{F_{el}^A}{k_B T} = \frac{\pi^2 R^2}{16 N_A a^2} \quad (4)$$

The B blocks are confined between two LC layers, Figure 3a. On one hand, they are compressed if the thickness h is less than the Gaussian size of the backbone section (spacer) connecting two neighbor side groups. The spacer consists of $m = N_B/N_C = 1/\phi$ segments and inequality $h \leq a\sqrt{m}$ is fulfilled if the fraction of the side groups is not too small,

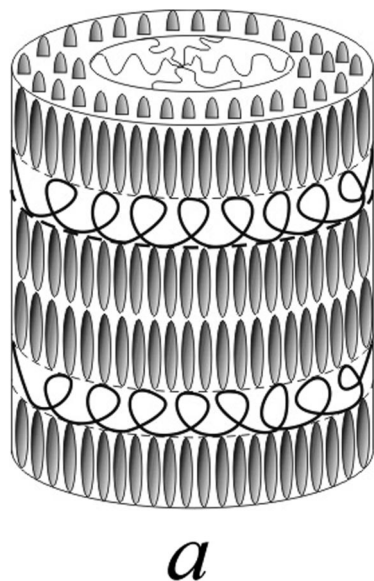
$$\phi \geq (v/a\sigma)^2 = (v/a^3)^{2/3}(v^{2/3}/\sigma)^2 \quad (5)$$

The first multiplier in the right-hand side of eq 5 describes flexibility of the chain: it is always less than the unity even for flexible chains.²⁵ The second multiplier is the ratio of the cross-area of the segment (bead) to the one of the side group. Usually, this ratio is also less than unity and inequality 5 means that if the fraction of the side groups is higher than some small value, the spacers of the B block (and the whole block) are compressed between the LC groups.

On the other hand, the B blocks are subjected to the radial stretching. Let us suppose that the free ends of the B blocks are located at the boundary of the Wigner-Seitz cell. The elastic free energy F_{el}^B can be written as

$$\frac{F_{el}^B}{k_B T} = \frac{3}{2a^2} \int_R^{R_0} dr E(r) \quad (6)$$

where the local stretching of the block $E(r) = dr/dn$ (derivative of the radial coordinate, r , $R < r < R_0$, over the number of segments, n) depends on the coordinate. This dependence can be found from the condition of dense packing of B monomer units: a thin ring of the width dr contains $Q dn$ segments so that $2\pi r dr h = Q dn v$. Therefore,



$$\frac{F_{el}^B}{k_B T} = \frac{3}{2a^2} \int_R^{R_0} dr \frac{Qv}{2\pi rh} = \frac{3R^2}{8a^2 N_A} (1 + n\phi) \times \ln \left(1 + \frac{N_B}{N_A} (1 + n\phi) \right) \quad (7)$$

where the space filling conditions, eq 3, are used.

The fourth term in eq 1 is responsible for a loss of conformational entropy of the spacers of the B block because of compression between two smectic layers. To estimate the entropic loss, let us imagine each spacer as a set of blobs, each of the size h containing g segments. Within the blob, the subchain of g links is Gaussian, $h \sim ag^{1/2}$, and does not "feel" confinement. A contribution of one blob to the entropy is of the order of unity. Keeping in mind that each spacer contains m/g blobs and the B block contains N_B/m spacers, we find that $F_{conf}/k_B T \sim (m/g)(N_B/m) \sim N_B a^2/h^2$. Numerical coefficient in the confinement free energy can be calculated if we use the so-called ground-state approximation²⁵ where the energy per segment is the minimum eigenvalue λ of the differential equation:

$$\frac{a^2}{6} \frac{\partial^2 \psi(x)}{\partial x^2} + \lambda \psi(x) = 0, \quad \frac{\partial \psi(x)}{\partial x} \Big|_{x=\pm h/2} = 0, \quad -\frac{h}{2} \leq x \leq \frac{h}{2} \quad (8)$$

The boundary conditions at the surfaces of the B layer ensure the constant density of monomer units throughout the layer. The solution of eq. 8 is chosen from the condition that it should be symmetric with respect to the origin of coordinates (middle of the layer), i.e. $\psi(x) = \text{const} \times \cos(x(6\lambda)^{1/2}/a)$. Thus, the confinement free energy per chain takes the following form

$$\frac{F_{conf}}{k_B T} = N_B \lambda = \frac{2\pi^2 N_B a^2}{3 h^2} = \frac{\pi^2}{6} N_B \phi^2 \left(\frac{a\sigma}{v} \right)^2 \quad (9)$$

Finally, the last term in eq 1 is the mixing free energy of the side groups. It is a combinatorial contribution accounting for a number of possible ways to create certain upper-bottom distribution of the side groups with respect to the backbone (B block). If the fraction of the upper LC groups is β , then

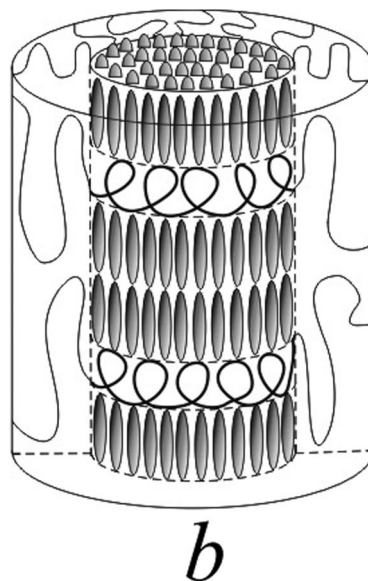


Figure 3. Each macromolecule of the amorphous (a) and liquid crystalline (b) cylinders participates in formation of two smectic monolayers separated by amorphous B layer.

$$\frac{F_{\text{mix}}}{k_B T} = N_C(\beta \ln \beta + (1 - \beta) \ln(1 - \beta)) \quad (10)$$

This contribution has a minimum at $\beta = 1/2$. Keeping in mind that the smectic layers formation imposes either $\beta = 1$ or $\beta = 1/2$, we conclude that the symmetric distribution of the side groups in the cylindrical structure is more favorable because $F_{\text{el}}^{\text{A,B}}$ and F_{int} do not depend on the distribution of the LC groups, whereas F_{conf} has a smaller value at the symmetric distribution of the LC groups (due to the larger thickness h at $\beta = 1/2$). Therefore

$$\frac{F_{\text{mix}}}{k_B T} = -\phi N_B \ln 2 \quad (11)$$

The equilibrium free energy of the cylindrical structure is calculated via minimization of $F_{\text{cyl}}^{\text{amorph}}$ over R :

$$\begin{aligned} \frac{F_{\text{cyl}}^{\text{amorph}}}{k_B T} &= \frac{\pi^2}{6} N_B \phi^2 \left(\frac{a\sigma}{v}\right)^2 + \phi N_B \left(\gamma_{\text{BC}} \frac{a\sigma}{v} - \ln 2\right) + \\ &3 \left(N_A \frac{(\gamma_{\text{AB}} + \gamma_{\text{AC}} n\phi)^2}{(1 + n\phi)^2} \left[\frac{\pi^2}{16} + \frac{3}{8}(1 + n\phi) \times \right. \right. \\ &\quad \left. \left. \ln \left(1 + (1 + n\phi) \frac{N_B}{N_A} \right) \right] \right)^{1/3}, \\ R &= a N_A^{2/3} \times \\ &\left(\frac{\gamma_{\text{AB}} + \gamma_{\text{AC}} n\phi}{(1 + n\phi) \left[\frac{\pi^2}{16} + \frac{3}{8}(1 + n\phi) \ln \left(1 + (1 + n\phi) \frac{N_B}{N_A} \right) \right]} \right)^{1/3} \quad (12) \end{aligned}$$

2.2. LC Cylinders and A \perp B Lamellae. The sketch of the structure of the cylinder with liquid crystalline core and amorphous corona is shown in Figure 3b. Similar to the amorphous cylinders, we assume that the LC groups are aligned parallel to the cylinder axis. The total free energy of the LC cylinders, $F_{\text{cyl}}^{\text{LC}}$, has the same structure as eq 1 and calculations of each contribution to the total free energy are straightforward. The equilibrium free energy is expressed as

$$\begin{aligned} \frac{F_{\text{cyl}}^{\text{LC}}}{k_B T} &= \frac{\pi^2}{6} N_B \phi^2 \left(\frac{a\sigma}{v}\right)^2 + \phi N_B \left(\gamma_{\text{BC}} \frac{a\sigma}{v} - \ln 2\right) + \\ &3 \left(N_B (\gamma_{\text{AB}} + \gamma_{\text{AC}} n\phi)^2 \left[\frac{\pi^2}{16} + \frac{3}{8(1 + n\phi)} \times \right. \right. \\ &\quad \left. \left. \ln \left(1 + \frac{1}{(1 + n\phi)} \frac{N_A}{N_B} \right) \right] \right)^{1/3} \quad (13) \end{aligned}$$

An analog of the lamellar structure of amorphous AB diblock copolymers in case of the ABC copolymers with LC side groups looks like in Figure 2c. Here amorphous A and B layers have perpendicular orientations and form square grid.

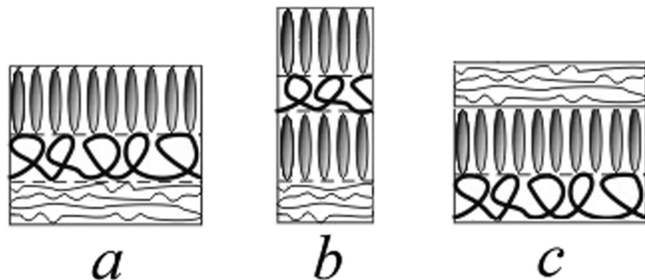


Figure 4. Conformations of macromolecules in BAB (a), A-B-B (b), and A-B-A (c) lamellar structures.

The interfacial energy of the lamellar structure differs from eq 2 by a numerical factor in the second term:

$$\frac{F_{\text{int}}}{k_B T} = \gamma_{\text{BC}} \phi N_B \frac{a\sigma}{v} + \frac{a N_A \gamma_{\text{AB}} + n\phi \gamma_{\text{AC}}}{R(1 + n\phi)} \quad (14)$$

Here R is the semithickness of the A layer. The free energy of stretching of A and B blocks can be calculated as for the case of diblock copolymers²⁴

$$\begin{aligned} \frac{F_{\text{el}}}{k_B T} &= \frac{F_{\text{el}}^{\text{A}} + F_{\text{el}}^{\text{B}}}{k_B T} = \frac{\pi^2}{8} \frac{R^2}{a^2 N_A} + \frac{\pi^2}{8} \frac{\rho^2}{a^2 N_B} = \\ &\frac{\pi^2}{8} \frac{R^2}{a^2 N_A} \left(1 + (1 + n\phi)^2 \frac{N_B}{N_A} \right) \quad (15) \end{aligned}$$

where ρ is the semithickness of the LC lamellae. All other contributions to the total free energy of the lamellae coincide with those for the cylindrical structures. The equilibrium free energy of the lamellar structure is calculated by minimization over R :

$$\begin{aligned} \frac{F_{\text{lam}}^{\text{A,B}}}{k_B T} &= \frac{\pi^2}{6} N_B \phi^2 \left(\frac{a\sigma}{v}\right)^2 + \phi N_B \left(\gamma_{\text{BC}} \frac{a\sigma}{v} - \ln 2\right) + \\ &3 \left(N_A \frac{(\gamma_{\text{AB}} + \gamma_{\text{AC}} n\phi)^2}{(1 + n\phi)^2} \frac{\pi^2}{32} \left(1 + (1 + n\phi)^2 \frac{N_B}{N_A} \right) \right)^{1/3} \quad (16) \end{aligned}$$

2.3. BAB Lamellae. If incompatibility of amorphous A blocks with the LC groups is high enough, one can expect stability of parallel layers where A and C species do not contact with each other, i.e., the periodical structure includes alternating BAB amorphous layers and smectic double layers, Figure 2d. In such structure, each macromolecule adopts conformation depicted in Figure 4a. All LC groups of the macromolecule participate in formation of one smectic monolayer, i.e., they are located on one side with respect to the backbone (B block). After the B layer, A blocks form half of the A layer and then the structure follows an inverse order: the second half of A layer, B layer and C monolayer. The CBABC element of the periodical structure corresponds to one period. Both A and B blocks are not stretched in the plane of the layers. If the fraction of the LC groups is high enough, the B block is squeezed between C and A layers, whereas A block can be either squeezed or stretched between two B layers. The stretching is realized if the length of the A block is high enough. Let us denote by S the area of the layer formed by one macromolecule. Then the dense packing conditions for each component take the form

$$SH = vN_A, \quad Sh = vN_B, \quad Sd = \sigma d N_C \quad (17)$$

where H and h are semithickness and thickness of A and B layers, respectively:

$$h = \frac{v}{\sigma\phi}, \quad H = \frac{vN_A}{\sigma\phi N_B} \quad (18)$$

The total free energy of the BAB lamellae includes contributions coming from the energy of interfaces

$$\frac{F_{\text{int}}}{k_B T} = (\gamma_{\text{AB}} + \gamma_{\text{BC}}) \frac{Sa}{v} \quad (19)$$

from the confinement free energy of B block

$$\frac{F_{\text{conf}}}{k_B T} = \frac{2\pi^2 N_B a^2}{3 h^2} \quad (20)$$

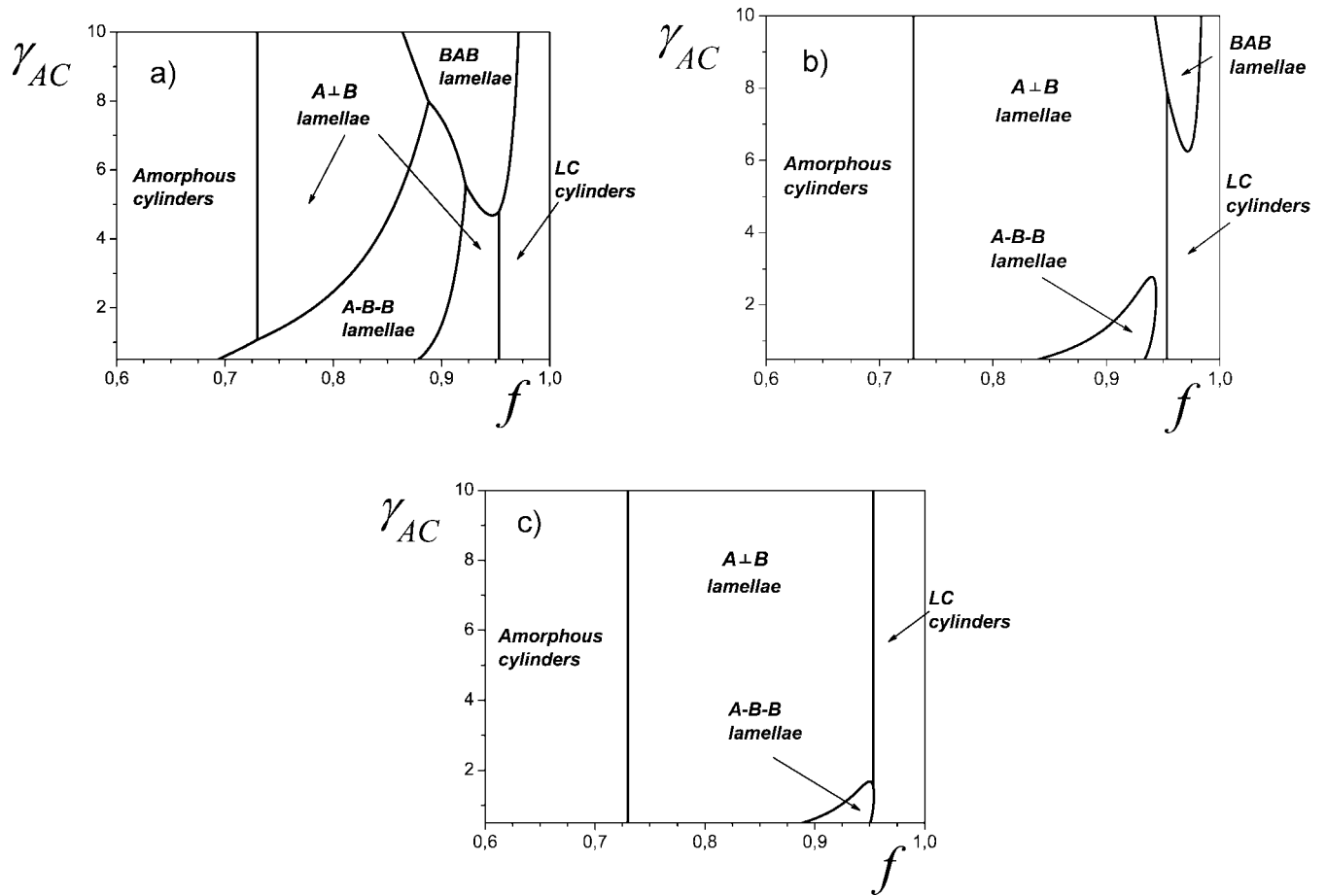


Figure 5. f - γ_{AC} phase diagrams for different values of the number of A and B segments in the block copolymer: $N = 100$ (a), 300 (b), and 500 (c). $\phi = 1/4$, $\gamma_{AB} = 0.5$, $n = 10$, and $a\sigma/v = 3$.

and from the entropic penalties of the A block

$$\frac{F_{ent}}{k_B T} = \frac{2\pi^2 N_A a^2}{3 \cdot 4H^2} + \frac{\pi^2 H^2}{8 a^2 N_A} \quad (21)$$

The latter expression is an interpolation form where the first term is responsible for squeezing at $H \ll aN_A^{1/2}$ and the second term is dominant when the A block is stretched, $H \gg aN_A^{1/2}$. The factor 4 in denominator of eq 21 means that the block is confined in the layer of the thickness $2H$. It has to be noticed that the mixing entropy, eq. 10, is equal to zero because all LC groups are located on one side with respect to the backbone ($\beta = 1$). Thus, the total free energy of the BAB lamellae takes the following form:

$$\frac{F_{lam}^{BAB}}{k_B T} = (\gamma_{AB} + \gamma_{BC})N_B \phi \frac{a\sigma}{v} + \frac{2\pi^2}{3} N_B \phi^2 \left(\frac{a\sigma}{v}\right)^2 \left(1 + \frac{N_B}{4N_A}\right) + \frac{\pi^2}{8} \left(\frac{v}{a\sigma}\right)^2 \frac{N_A}{\phi^2 N_B^2} \quad (22)$$

2.4. A-B-B and A-B-A Lamellae. If incompatibility of amorphous A and B blocks with each other is high enough, one can expect stability of parallel layers where A and B species do not contact with each other, i.e., the periodical structure includes alternating pure amorphous layers of A and B kinds which are separated by smectic layers, Figure 2e,f. In such structures, the sequence of the amorphous layers can look either like A-B-B-A-B-B-... or like A-B-A-B-..., and each macromolecule adopts conformations depicted in parts b and c

of Figure 4, respectively. In other words, in the case of the structure in Figure 4b, the LC groups of the macromolecule are distributed symmetrically with respect to the backbone (B block), whereas A block passes through one of the smectic monolayers and forms half of the A layer. The dense packing conditions

$$SH = vN_A, \quad Sh = vN_B, \quad Sd = \sigma d \frac{N_C}{2} \quad (23)$$

indicate that the amorphous layers are twice thicker than those in the BAB lamellae, $h = 2v/(\sigma\phi)$, $H = 2vN_A/(\sigma\phi N_B)$, because of smaller area per molecule, S . The total free energy of the A-B-B lamellae has similar structure as eq 22:

$$\frac{F_{lam}^{A-B-B}}{k_B T} = \left(\frac{\gamma_{AC}}{2} + \gamma_{BC}\right)N_B \phi \frac{a\sigma}{v} + \frac{\pi^2}{6} N_B \phi^2 \left(\frac{a\sigma}{v}\right)^2 \left(1 + \frac{N_B}{4N_A}\right) + \frac{\pi^2}{2} \left(\frac{v}{a\sigma}\right)^2 \frac{N_A}{\phi^2 N_B^2} - N_B \phi \ln 2 \quad (24)$$

where the last term corresponds to the mixing entropy of the side groups. It has to be noted that eq. 24 does not take into account interaction energy of the LC groups with a spacer (a segment of the A block of the length d) which connects the B block with the A layer. This contribution $\sim \gamma_{AC} a d v^{2/3}$ is negligible in comparison with the first term of eq. 24.

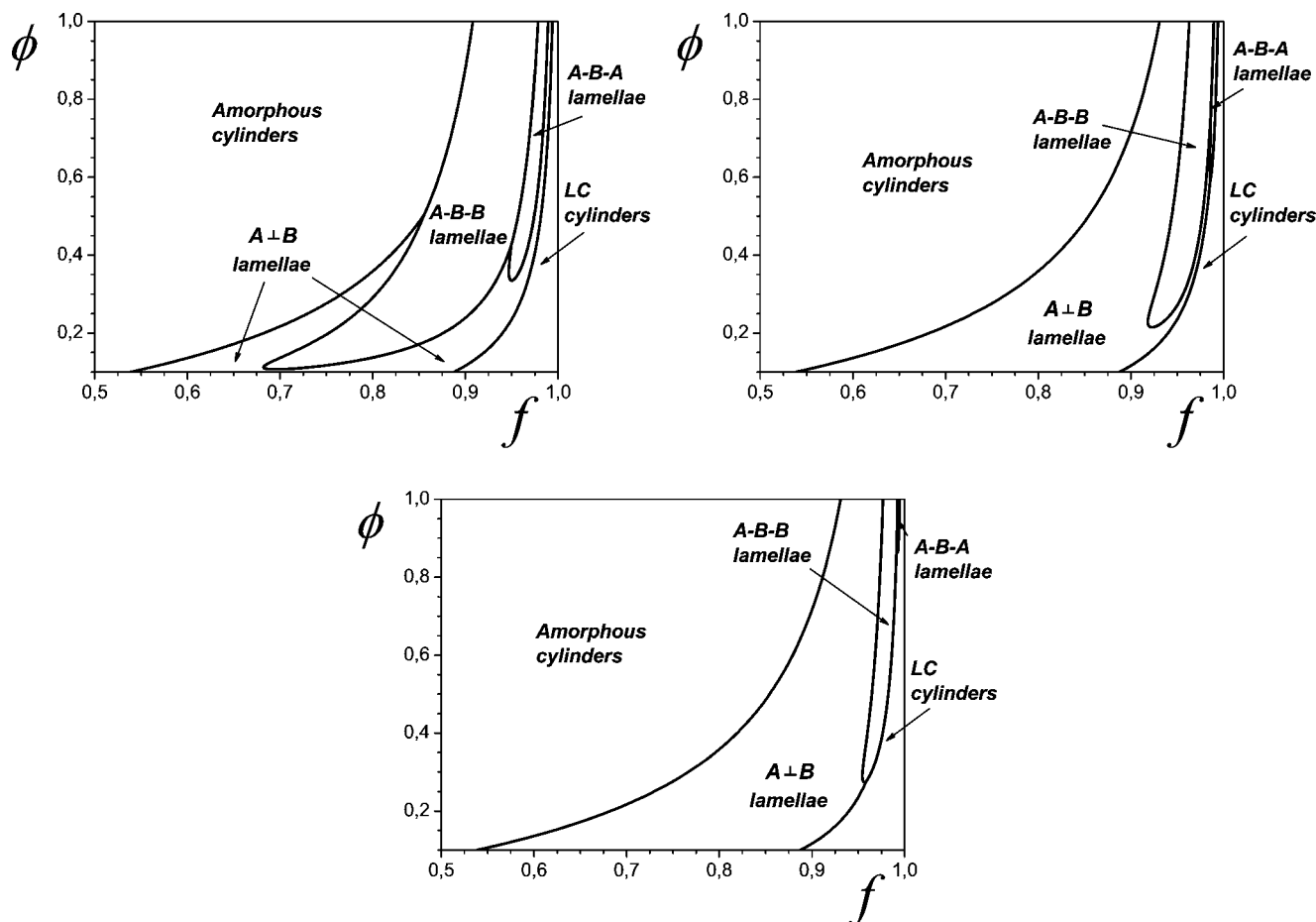


Figure 6. f – ϕ phase diagrams for different values of the number of A and B segments in the block copolymer: $N = 100$ (a), 300 (b), and 500 (c). $\gamma_{AC} = 2$, $\gamma_{AB} = 0.5$, $n = 10$, and $a\sigma v = 3$.

Similar to eq. 22, the total free energy of the A–B–A lamellae takes the form:

$$\frac{F_{\text{lam}}^{\text{A-B-A}}}{k_B T} = (\gamma_{AC} + \gamma_{BC})N_B \phi \frac{a\sigma}{v} + \frac{\pi^2}{6} N_B \phi^2 \left(\frac{a\sigma}{v} \right)^2 \left(1 + \frac{N_B}{N_A} \right) + \frac{\pi^2}{8} \left(\frac{v}{a\sigma} \right)^2 \frac{N_A}{\phi^2 N_B^2} \quad (25)$$

3. Results and Discussion

The phase diagrams of the melt of the AB diblock copolymers with liquid crystalline side groups are constructed via numerical solution of equations $F_{\text{cyl}}^{\text{amorph}} = F_{\text{lam}}^{\text{ALB}}$, $F_{\text{cyl}}^{\text{LC}} = F_{\text{lam}}^{\text{ALB}}$, etc., where the free energies of all possible morphologies, eqs 12, 13, 16, 22, 24, and 25 are analyzed. Comparison of the free energies of different structures enables us to conclude that phase behavior of the system does not depend on the surface tension coefficient γ_{BC} (assuming that it is just high enough to provide the strong segregation regime) because γ_{BC} comes into each expression of the free energy only as a combination $\gamma_{BC}\phi N_B$. The parameters controlling phase behavior are γ_{AB} , γ_{AC} , n , ϕ , f , and N . In all our calculations we fix the values of the surface tension coefficient $\gamma_{AB} = 0.5$, the dimensionless volume of the side group $n = 10$, and the parameter $a\sigma v = 3$. Such choice of γ_{AB} , which can be expressed through the Flory–Huggins parameter χ_{AB} as $\gamma_{AB} = \sqrt{\chi_{AB}/6}$ provides the strong segregation condition, $\chi_{AB}N \gg 1$, for all considered values of N : 100, 300, and 500.

The f – χ_{AC} phase diagrams in Figure 5 are plotted at $\phi = 1/4$ and different values of N : 100 (a) 300 (b), and 500 (c). Similar

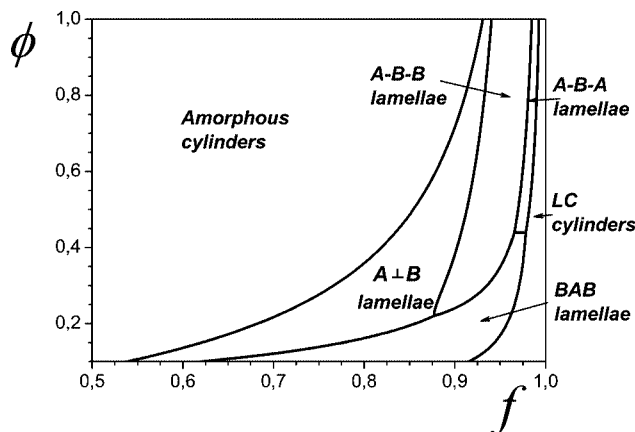


Figure 7. f – ϕ phase diagram. $N = 100$, $\gamma_{AC} = 7$, $\gamma_{AB} = 0.5$, $n = 10$, $a\sigma v = 3$.

to the conventional diagram for the melt of diblock copolymers, the amorphous cylinders are stable if the A block is shorter than the B block whereas transition to the A \perp B lamellae (an analogue of the lamellar structure of AB copolymer) occurs at $f > 1/2$, Figure 5. Such a shift is related to the presence of the LC groups which make the effective excluded volume of the B block larger. In other words, one can say that the presence of the side groups effectively “elongates” the B block. The LC cylinders (an inverse cylindrical structure) are stable with the increase of the fraction f . Both *amorphous cylinders*–A \perp B lamellae and A \perp B lamellae–LC cylinders transitions do not depend on the surface tension coefficient γ_{AC} (the corresponding

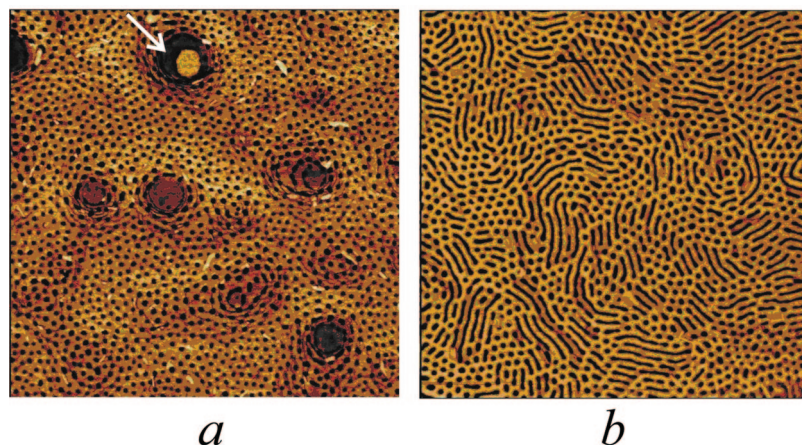


Figure 8. SFM phase images of complexes of P2VP₁₈₀-*b*-PEO₅₆₀ diblock copolymers with wedge-shaped molecules after 3 days benzene vapor annealing.¹⁶ The images differ by the fraction of the liquid crystalline groups complexed with the P2VP block: $\phi = 0.58$ (a), and 0.22 (b). Scan size is $2 \times 2 \mu\text{m}^2$. Reproduced with permission from ref 16. Copyright 2009 American Chemical Society.

boundaries in Figure 5 are straight lines). This result is also a demonstration of the analogy with the strong segregation regime in AB copolymers: a combination $\gamma_{\text{eff}} = \gamma_{\text{AB}} + \gamma_{\text{AC}}n\phi$ comes into eqs. 12, 13, 16 as $\gamma_{\text{eff}}^{2/3}$ and does not contribute to the expressions for equality of the corresponding free energies. The BAB and A-B-B lamellae are stable if the molecules are short enough, Figure 5a. The increase of N narrows stability regions of the BAB and A-B-B lamellae, Figure 5bc, and they are unstable in the limit of $N \rightarrow \infty$. Such behavior is related to different dependence of the total free energies of various structures on N . All contributions to the total free energies of the BAB and A-B-B lamellae have linear dependence on N (except for the stretching free energy) and the free energies are positive, eqs. 22, 24. On the other hand, the elastic free energies and interfacial energies of the amorphous, LC cylinders and A \perp B lamellae have weaker dependence, $\sim N^{1/3}$, eqs 12, 13, and 16. Therefore, one can achieve conditions when the decrease of N results in drastic decrease of $F_{\text{lam}}^{\text{BAB}}$ and $F_{\text{lam}}^{\text{A-B-B}}$ with respect to $F_{\text{cyl}}^{\text{amorph}}$, $F_{\text{cyl}}^{\text{LC}}$, and $F_{\text{lam}}^{\text{A} \perp \text{B}}$. It is natural that A-B-B lamellae are stable at smaller values of γ_{AC} whereas the BAB lamellae, which do not have A-C contacts, remain stable only at higher values. The A-B-B lamellae are characterized by smaller confinement and mixing free energies than the BAB lamellae, eqs 22 and 24. That is why A-C contacts in the A-B-B lamellae become unfavorable only at high values of γ_{AC} , which promotes transition to the BAB lamellae. It has to be noted that in the f - γ_{AC} diagrams we do not analyze behavior of the copolymer in the close vicinity of the boundary values of f : 0 and 1. Here, the homogeneous structure of the copolymer has to stable.

The f - ϕ diagrams in Figure 6 are plotted at $\gamma_{\text{AC}} = 2$ and different values of N : 100 (a) 300 (b), and 500 (c). Due to relatively low value of the surface tension coefficient γ_{AC} , the BAB lamellae are not stable at any values of the fraction ϕ . In all cases the increase of the fraction of the side groups, ϕ , widens stability region of the amorphous cylinders and narrows stability regions of all other structures. The A-B-A lamellae are stable only at relatively high values of f , i.e., under the condition that the A blocks are stretched. Keeping in mind that the A-B-B lamellae are characterized by higher mixing entropy of the side groups and smaller interfacial energy, eqs 24 and 25, the natural question is why the A-B-A lamellae can have smaller free energy than the A-B-B ones. The stability of the A-B-A lamellae is provided by the stretching free energy of the A blocks. The A blocks in the A-B-A lamellae are less stretched because the area of AC interface per molecule is larger than in the A-B-B lamellae. Figure 6 shows that variation of the

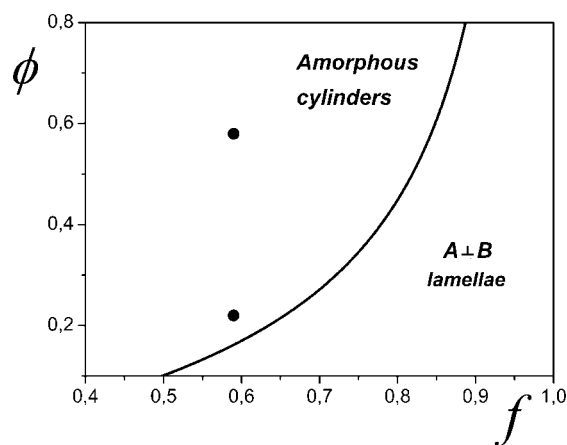


Figure 9. Two phases in the f - ϕ phase diagram. The boundary between the phases is obtained for $n = 8$. Upper and bottom points correspond to the SFM phase images of Figure 8, parts a and b, respectively.

parameter ϕ can be responsible for morphological transitions. The effect of N is also clear seen in Figure 6. Increasing N gradually suppresses stability of the A-B-B and A-B-A lamellae.

The f - ϕ diagram in Figure 7 demonstrates the stability of the BAB lamellae for the case of relatively short polymer chains, $N = 100$, and high incompatibility of A blocks with the side groups, $\gamma_{\text{AC}} = 7$. This structure can exist only if the grafting density of the side groups is low enough.

3.1. Comparison with Experimental Data. Our theoretical predictions for the transition between amorphous cylinders and A \perp B lamellae are consistent with recent experimental results.¹⁶ In ref.¹⁶ wedge-shaped molecules with a sulfonic group at the tip have been incorporated into a poly(2-vinylpyridine)-*b*-poly(ethylene oxide) (P2VP-*b*-PEO) diblock copolymer via proton transfer at different degrees of neutralization. The thin film morphology of the complexed block copolymers has been studied by scanning force microscopy (SFM) and X-ray reflectivity. The complexes exhibited strongly segregated patterns comprising smectic layers of the complexed P2VP blocks, oriented parallel to the substrate throughout the whole film with the embedded PEO domains. For the complexes with a degree of neutralization of $\phi \approx 0.58$ ordered amorphous PEO cylinders were observed oriented perpendicular to the substrate. For a degree of neutralization equal to 0.22 initially also perpendicular PEO cylinders were formed, but upon solvent-vapor annealing they partially merged, resulting in a mixed lamellar-cylindrical

morphology, Figure 8. The SFM images allowed to detect the increase of the diameter of the PEO cylinders with the decrease of the degree of neutralization: $2R \approx 22 \pm 2$ nm at $\phi = 0.58$ and $2R \approx 28 \pm 2$ nm at $\phi = 0.22$. On the contrary, the distance between the cylinders remains approximately the same:¹⁶ $2R_0 \approx 46 \pm 3$ nm at $\phi = 0.22$ and $2R_0 \approx 48 \pm 4$ nm at $\phi = 0.58$.

To interrelate our modeling parameters with the experimental ones, we used data from Table 1 in ref 16. Noncomplexed P2VP₁₈₀-*b*-PEO₅₆₀ diblock copolymers were found to have a fraction of PEO equal to 0.59. Taking into account that always the same diblock copolymers were used for complexation with LC groups, one can expect that $f = N_A/(N_A + N_B) \approx 0.59$. In Table 1 in ref 16, the fraction of PEO in the complexed copolymers, Φ_{PEO} , has values $\Phi_{\text{PEO}} = 0.34, 0.2,$ and 0.14 at the degree of neutralization (fraction of the side groups, $\phi = N_C/N_B$) $\phi = 0.22, 0.58, 1,$ respectively. In our model, Φ_{PEO} is determined as

$$\Phi_{\text{PEO}} = \frac{N_A v}{N_A v + N_B v + N_C \sigma d} = \frac{f}{1 + \phi n(1 - f)} \quad (26)$$

Substitution of three different values of Φ_{PEO} and ϕ into this equation gives us three different values of the parameter n : 8.15, 8.2, and 7.84. Thus, we can assume that the average relative volume of the side group is $n \approx 8$. The cylinder-to-lamellae transition is calculated by equation $F_{\text{cyl}}^{\text{amorph}} = F_{\text{lam}}^{\text{ALB}}$:

$$\frac{\pi^2}{16} + \frac{3}{8}(1 + n\phi) \ln\left(1 + \frac{(1 - f)(1 + n\phi)}{f}\right) = \frac{\pi^2}{32} \left(1 + \frac{(1 - f)(1 + n\phi)^2}{f}\right) \quad (27)$$

where n has to be set equal to 8. The f - ϕ diagram (solution of eq 27, solid line) and two points corresponding to the SFM images of Figure 8a (upper point) and Figure 8b (bottom point) are presented in Figure 9. We can see that the upper point is located far from the transition line what can explain thermodynamic stability of the cylindrical structure shown in Figure 8a. On the other hand, the bottom point is located in pretransitional region, and coexistence of the cylindrical and lamellar structures, Figure 8b, is quite natural.

The decrease of the radius of the PEO cylinder with ϕ is related to the decrease of the aggregation number of the cylinder. Indeed, the increase of ϕ corresponds to additional stretching of the P2VP block and to the increase of the excluded volume of the blocks forming corona of the cylinder. The ratio of the radii of the cylinders with different fraction of the LC groups, $R_{0.22}/R_{0.58}$, can be calculated using eq. 12. In addition to $n, f,$ and ϕ , this ratio depends on the ratio of the surface tension coefficients, $t = \gamma_{\text{AC}}/\gamma_{\text{AB}}$. However, $R_{0.22}/R_{0.58} > 1$ at any values of t . For example, $R_{0.22}/R_{0.58} = 1.68$ and 1.214 at $t = 0$ and ∞ , respectively. The best fitting value of t corresponding to the experimental data $R_{0.22}/R_{0.58} \approx 1.273$ is $t \approx 2.1$. For the distance between the cylinders $D = 2R[1 + (1 - f)(1 + n\phi)/f]^{1/2}$, the value $t = 2.1$ gives also good agreement with the experiment:

$$\frac{D_{0.22}}{D_{0.58}} = 0.98 \quad \text{theory}$$

$$\frac{D_{0.22}}{D_{0.58}} = 0.96 \quad \text{experiment} \quad (28)$$

4. Conclusions

We have developed a strong segregation theory of microphase separation of linear AB block copolymers with liquid crystalline

side groups (C) attached to the B blocks. We predicted thermodynamic stability of direct and inverse cylindrical structures, Figure 2a,b, and four kinds of lamellar structures where the A and B amorphous layers have perpendicular orientations (so-called $A \perp B$ lamellae), Figure 2c, the BAB amorphous layers are segregated by the smectic double layers (BAB lamellae), Figure 2d, and pure A and B layers are segregated by the smectic ones and have sequences A-B-B-A-B-B-... (A-B-B lamellae), Figure 2e, or A-B-A-B-... (A-B-A lamellae), Figure 2f. Optimum conditions for the stability of the mentioned morphologies can be summarized as follows.

1. Amorphous Cylinders: long macromolecules; high fraction of the B and C (LC) units; any values of the surface tension coefficients satisfying the strong segregation conditions.

2. Liquid Crystalline Cylinders: long macromolecules; high fraction of the A units and small enough fraction of the liquid crystalline units; any values of the surface tension coefficients satisfying the strong segregation conditions.

3. $A \perp B$ Lamellae: long macromolecules; the A block has to be a bit longer than the B block; small enough fraction of the liquid crystalline units; any values of the surface tension coefficients satisfying the strong segregation conditions.

4. BAB Lamellae: short enough macromolecules; high fraction of the A units; small enough fraction of the liquid crystalline units; high values of the surface tension coefficient γ_{AC} .

5. A-B-B Lamellae: short enough macromolecules; high fraction of the A units; high enough fraction of the liquid crystalline units.

6. A-B-A Lamellae: short enough macromolecules; high fraction of the A units; high fraction of the liquid crystalline units.

Our theoretical predictions for amorphous cylinders and $A \perp B$ lamellae are quantitatively consistent with experimental data.

Acknowledgment. I.I.P. thanks Ahmed Mourran and Martin Möller for stimulating discussions. The financial support of the Deutsche Forschungsgemeinschaft within SFB 569, the Federal Agency for Science and Innovation (Russian Federation), and the Dynasty Foundation (Russian Federation) is gratefully acknowledged.

References and Notes

- (1) Ruokolainen, J.; Mäkinen, R.; Torkkeli, M.; Mäkelä, T.; Serimaa, R.; ten Brinke, G.; Ikkala, O. *Science* **1998**, *280*, 557.
- (2) Nap, R. J.; Kok, C.; ten Brinke, G.; Kuchanov, S. I. *Eur. Phys. J. E* **2001**, *4*, 515.
- (3) Nap, R. J.; ten Brinke, G. *Macromolecules* **2002**, *35*, 952.
- (4) Nap, R. J.; Erukhimovich, I. Ya.; ten Brinke, G. *Macromolecules* **2004**, *37*, 4296.
- (5) Smirnova, Yu. G.; ten Brinke, G.; Erukhimovich, I. Ya. *J. Chem. Phys.* **2006**, *124*, 054907.
- (6) Palyulin, V. V.; Potemkin, I. I. *Polym. Sci., Ser. A* **2007**, *49*, 473.
- (7) Palyulin, V. V.; Potemkin, I. I. *J. Chem. Phys.* **2007**, *127*, 124903.
- (8) Mao, G.; Wang, J.; Clingman, S. R.; Ober, C. K.; Chen, J. T.; Thomas, E. L. *Macromolecules* **1997**, *30*, 2556.
- (9) Hamley, I. W.; Castelletto, V.; Lu, Z. B.; Imrie, C. T.; Itoh, T.; Al-Hussein, M. *Macromolecules* **2004**, *37*, 4798.
- (10) Anthamatten, M.; Hammond, P. T. *Macromolecules* **1999**, *32*, 8066.
- (11) Osuji, C. O.; Chen, J. T.; Mao, G.; Ober, C. K.; Thomas, E. L. *Polymer* **2000**, *41*, 8897.
- (12) Verploegen, E.; McAfee, L. C.; Tian, L. T.; Verploegen, D.; Hammond, P. T. *Macromolecules* **2007**, *40*, 777.
- (13) Anthamatten, M.; Zheng, W. Y.; Hammond, P. T. *Macromolecules* **1999**, *32*, 4838.
- (14) Muthukumar, M.; Ober, C. K.; Thomas, E. L. *Science* **1997**, *277*, 1225.
- (15) de Jeu, W. H.; Séréro, Y.; Al-Hussein, M. *Adv. Polym. Sci.* **2006**, *200*, 71.
- (16) Albrecht, K.; Mourran, A.; Zhu, X.; Markkula, T.; Groll, J.; Beginn, U.; de Jeu, W. H.; Möller, M. *Macromolecules* **2008**, *41*, 1728.

- (17) Al-Hussein, M.; Séréro, Y.; Konovalov, O.; Mourran, A.; Möller, M.; de Jeu, W. H. *Macromolecules* **2005**, *38*, 9610.
- (18) Wong, G. C. L.; Commandeur, J.; Fischer, H.; de Jeu, W. H. *Phys. Rev. Lett.* **1996**, *77*, 5221.
- (19) Ansari, I. A.; Castelletto, V.; Mykhaylyk, T.; Hamley, I. W.; Lu, Z. B.; Itoh, T.; Imrie, C. T. *Macromolecules* **2003**, *36*, 8898.
- (20) Figueiredo, P.; Geppert, S.; Brandsch, R.; Bar, G.; Thomann, R.; Spontak, R. J.; Gronski, W.; Samlenski, R.; Müller-Buschbaum, P. *Macromolecules* **2001**, *34*, 171.
- (21) Verploegen, E.; Zhang, T.; Jung, Y. S.; Ross, C.; Hammond, P. T. *Nano Lett.* **2008**, *8*, 3434 .
- (22) Anthamatten, M.; Hammond, P. T. *J. Polym. Sci., Part B* **2001**, *39*, 2671.
- (23) Shah, M.; Pryamitsyn, V.; Ganesan, V. *Macromolecules* **2008**, *41*, 218.
- (24) Semenov, A. N. *Sov. Phys. JETP* **1985**, *61*, 733.
- (25) Grosberg, A. Yu.; Khokhlov, A. R. *Statistical Physics of Macromolecules*; AIP Press: New York, 1994.

MA802365Y